



Reconstruction of intracortical whisker-evoked local field potential from electrocorticogram using a model trained for spontaneous activity in the rat barrel cortex



Hidenori Watanabe^{a,*}, Tomoya Sakatani^a, Takafumi Suzuki^b, Masa-aki Sato^c, Yukio Nishimura^{a,d,e}, Atsushi Nambu^{e,f}, Mitsuo Kawato^g, Tadashi Isa^{a,e}

^a Department of Developmental Physiology, National Institute for Physiological Sciences, Okazaki, Aichi 444-8686, Japan

^b Center for Information and Neural Networks, National Institute of Information and Communications Technology, and Osaka University, Suita, Osaka 565-0871, Japan

^c Advanced Telecommunications Research Institute International, Neural Information Analysis Laboratory, Soraku, Kyoto 619-0288, Japan

^d Precursory Research for Embryonic Science and Technology, Japan Science and Technology Agency, Chiyoda, Tokyo 102-8666, Japan

^e The Graduate University for Advanced Studies, Hayama, Kanagawa 240-0193, Japan

^f Department of Integrative Physiology, National Institute for Physiological Sciences, Okazaki, Aichi 444-8686, Japan

^g Advanced Telecommunications Research Institute International, Computational Neuroscience Laboratory, Soraku, Kyoto 619-0288, Japan

ARTICLE INFO

Article history:

Received 15 April 2014

Received in revised form 25 June 2014

Accepted 27 June 2014

Available online 7 July 2014

Keywords:

Micro-ECoG

LFP

Decoding

Current source density

Sparse linear regression

BMI

ABSTRACT

Electrocorticogram (ECoG) has provided neural information from the cortical surfaces, is widely used in clinical applications, and expected to be useful for brain–machine interfaces. Recent studies have defined the relationship between neural activity in deep layers of the cerebral cortex and ECoG. However, it is still unclear whether this relationship is shared across different brain states. In this study, spontaneous activity and whisker-evoked responses in the barrel cortex of anesthetized rats were recorded with a 32-channel ECoG electrode array and 32-channel linear silicon probe electrodes, respectively. Spontaneous local field potentials (LFPs) at various depths could be reconstructed with high accuracy ($R > 0.9$) by a linear weighted summation of spontaneous ECoG. Current source density analysis revealed that the reconstructed LFPs correctly represented laminar profiles of current sinks and sources as well as the raw LFP. Moreover, when we applied the spontaneous activity model to reconstruction of LFP from the whisker-related ECoG, high accuracy of reconstruction could be obtained ($R > 0.9$). Our results suggest that the ECoG carried rich information about synaptic currents in the deep layers of the cortex, and the same reconstruction model can be applied to estimate both spontaneous activity and whisker-evoked responses.

© 2014 Elsevier Ireland Ltd and the Japan Neuroscience Society. All rights reserved.

1. Introduction

Electrocorticogram (ECoG), which is measured from the cortical surface, has been proposed as a useful primary control signal for brain–machine interfaces (BMIs), because they have been shown to provide rich information about motor outputs in both human and non-human primate (Waldert et al., 2009; Yanagisawa et al., 2011,

2012a; Shin et al., 2012; Chen et al., 2013). Similar to use of ECoG in motor output systems, ECoG can detect neural responses about sensory inputs in the visual cortices (e.g., Lachaux et al., 2005; Toda et al., 2011; Majima et al., 2014), in the auditory cortices (e.g., Crone et al., 2001; Edwards et al., 2005; Trautner et al., 2006; Fukushima et al., 2012), in the olfactory bulbs of rabbits (Freeman and Baird, 1987), in the auditory and somatosensory cortices (e.g., Ray et al., 2008a), and the sensorimotor cortices (e.g., Crone et al., 1998; Miller et al., 2009; Yanagisawa et al., 2012b). On the other hand, intracortical local field potentials (LFPs) have been shown to carry substantial information about sensory inputs or motor outputs, because LFPs include both synaptic potentials and spiking activities of a large number of neurons around the recording electrode (Mitzdorf, 1985; Katzner et al., 2009; Lindén et al., 2011). To identify how much information about the intracortical activity can be recorded from

Abbreviations: ECoG, electrocorticogram; LFP, local field potential; CSD, current source density; BMI, brain–machine interface; SLiR, sparse linear regression.

* Corresponding author at: National Institute for Physiological Sciences, 38 Nishigonaka Myodaiji, Okazaki, Aichi 444-8585, Japan. Tel.: +81 564 55 7763; fax: +81 564 55 7766.

E-mail address: watanabe@nips.ac.jp (H. Watanabe).

<http://dx.doi.org/10.1016/j.neures.2014.06.010>

0168-0102/© 2014 Elsevier Ireland Ltd and the Japan Neuroscience Society. All rights reserved.

the cortical surface, it is necessary to investigate the relationship between the ECoG signals and intracortical LFPs.

Recently, some studies have shown the relationship between the ECoG signals and intracortical neuronal activity. Visual stimulation to individual eye simultaneously induced evoked ECoG signals and larger amplitudes of intracortical LFPs and change of firing rate in rat visual cortex (Toda et al., 2011). Change of firing rate or synchronization of intracortical neural population were reflected in modulation of high gamma power in the ECoG signal of macaque secondary somatosensory cortex (Ray et al., 2008b) and rats (Yazdan-Shahmorad et al., 2013). We demonstrated a spatiotemporal relationship between ECoG and LFP signals in the primary motor cortex of a behaving macaque monkey using a computational approach (Watanabe et al., 2012). Our work revealed that a linear weighted summation of the ECoG signals carries information of LFP using a sparse linear regression (SLiR) algorithm. The set of weights in this linear regression describes a relationship between ECoG and deeper layer LFP signals. However, it is still unclear whether this relationship is shared across various brain states. To address this question, spontaneous activity and whisker-evoked responses were recorded with ECoG on cortical surface, and the deep layer LFPs by needle electrodes in the barrel cortex of anesthetized rats. Then we attempted to reconstruct whisker-evoked LFPs using the weight coefficient obtained through reconstruction of the spontaneous LFPs. A current source density (CSD) analysis was used to determine whether the reconstructed LFPs carried appropriate information about the synaptic events in the cortical layers. If the weight coefficient of a decoder for spontaneous LFPs successfully reconstructed the whisker-evoked LFPs, it would suggest a shared mechanism of processing in the cortical circuits across different brain states.

2. Materials and methods

All experimental procedures were performed in accordance with the Guidelines for Proper Conduct of Animal Experiments of the Science Council of Japan and approved by the Committee for Animal Experiment at the National Institutes of Natural Sciences (Approval No.: 11A158).

2.1. Structure of the ECoG electrodes

An electrode-mesh (Fig. 1A) was designed to contain 32 ECoG electrodes with an inter-electrode distance of 0.4 mm. The 3 mm × 3 mm mesh was constructed from Parylene-C (Poly (chloro-para-xylylene)) (Watanabe et al., 2012), and 5 × 5 square holes (200 μm × 200 μm each) were opened in the space between the electrodes. The center-to-center and side-to-side distance between adjacent holes were 0.4 mm and 0.2 mm, respectively (inset of Fig. 1A). The fabricated electrodes were arranged as a 6 × 6 grid, covering a 2 mm × 2 mm area. The electrodes at the four corners of the 6 × 6 grid were omitted. The gold surface of each electrode was exposed (50 μm × 50 μm). The electrical circuit was constructed from patterned gold that connected the 32 electrodes to 32 contact pads. Platinum-black coating of each electrode yielded an electronic impedance of 137 ± 223 kΩ (mean ± standard deviation) at 1 kHz.

2.2. Animal preparation for ECoG and LFP recordings

A schematic illustration of the recording setup is shown in Fig. 1B and C. Data were obtained from three adult male rats (Wistar, 300–400 g). The rats were anesthetized with intraperitoneal injections of urethane (Ethyl carbamate; Sigma-Aldrich Co. LLC, MO, USA; Product No. U2500; 0.5 ml of 20% solution/100 g body weight). During the surgery and the recording session,

animals were fixed to a stereotaxic apparatus. The depth of anesthesia was maintained at a constant level by monitoring hindpaw withdrawal reflexes and administering extra doses as necessary. Body temperature was maintained near 37 °C using a heating blanket (TCAT-2DF; Physitemp Instruments, Inc., NJ, USA). The left barrel cortex was exposed by a 6 mm × 6 mm craniotomy centered on a point 2.5 mm posterior and 5.5 mm lateral to bregma (Paxinos and Watson, 2007).

The electrode mesh was placed on the surface of the cortex after removal of the dura matter. A 32-channel microelectrode with an impedance of 0.5 MΩ (NeuroNexus technologies, USA) was inserted with a motor-driven micromanipulator (DMA-1511 and SM-11; Narishige, Tokyo, Japan) through the center of the electrode mesh into the cortex to record intracortical LFPs in combination with the ECoG signals (Fig. 1B). Two stainless steel screws for anchor and electrode reference of the ECoG array were implanted 2 mm rostral to the bregma.

2.3. Mechanical whisker stimulation

We developed a mechanical whisker-stimulation system based on miniature solenoid-driven actuators (Krupa et al., 2001). Mechanical stimulation of individual whiskers was performed with a custom-made piezoelectric actuator that provided movements via a ring-shaped metal wire (Fig. 1C). Our system stimulated 16 individual whiskers and enabled us to quickly identify a principal whisker within the recording site, which was arbitrarily determined. Each whisker (B1-4, C1-4, D1-4, E1-4) was cut approximately 2 cm from their base and slipped into a ring at the end of a stainless wire connected to the piezoelectric actuator. The discrete timing of stimulation was controlled by a custom-made software on LabVIEW (National Instruments, Austin, TX, USA). Each whisker was stimulated individually with a square pulse for 100 ms (Fig. 1D and a). Voltage was adjusted to produce movements 1 mm in amplitude in the dorsal direction.

2.4. Data acquisition

Multichannel ECoG and LFP signals were differentially amplified using a 64-channel amplifier (Cerebus; Blackrock Microsystems, UT, USA) with 2 kHz and 0.1 Hz high- and low-cutoff filters, respectively. Both ECoGs and intracortical neural activities were simultaneously recorded. Spontaneous activity in the barrel cortex was first recorded during the resting-state of the rat, and then neural signals in response to the whisker stimuli were recorded. During the 120 s recording session of whisker responses, each animal was exposed to repetitive deflections of the dominant whisker for the LFP recording at a frequency of 0.5 Hz (total 59 trials per session). The sampling frequency was 30 kHz. The LFPs and ECoGs were obtained by low-pass filtering (cutoff frequency: 300 Hz) and down-sampling (30 kHz to 1 kHz) of the wide-band-filtered signals. Offline data were analyzed using Matlab (Mathworks, USA).

2.5. Reconstruction of the intracortical LFPs from the ECoG signals

Estimation of the intracortical LFPs from ECoGs was performed using a sparse linear regression algorithm (SLiR; Nambu et al., 2009; Toda et al., 2011; Watanabe et al., 2012). The reconstructed LFP at depth d , u , at time t was described as:

$$u^d(t) = \sum_{i=1}^N \sum_{\delta=1}^T w_{i,\delta}^d x_i(t - \delta),$$

where $x_i(t - \delta)$ is the ECoG signal of channel i at time $(t - \delta)$ and $w_{i,\delta}^d$ is a weight coefficient from the i -th ECoG electrode with time

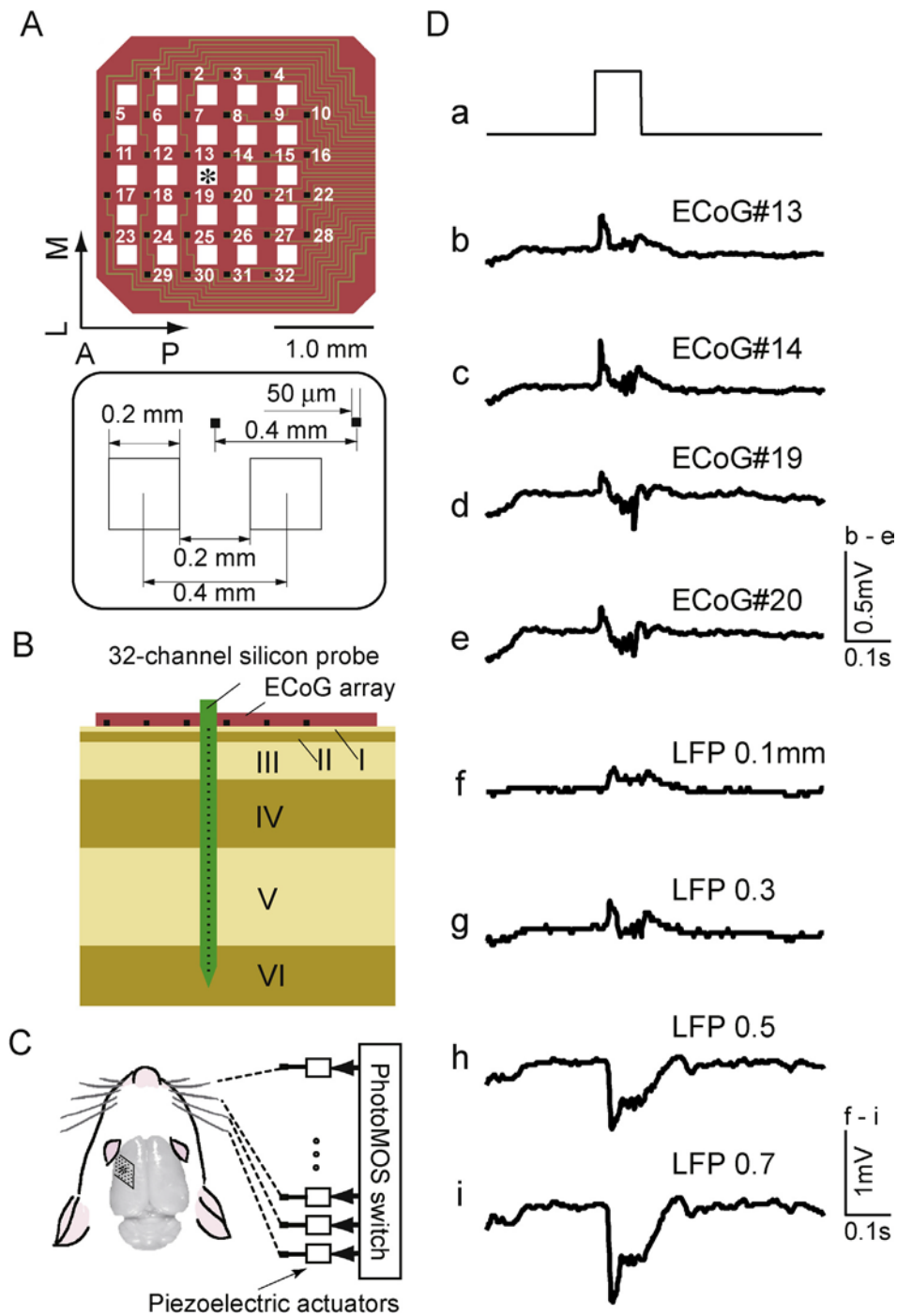


Fig. 1. Recording setup. (A) Structure of the poly ECoG array. The 32-channel electrodes (black squares, numbered 1–32) were manufactured from 20 μm -thick chloro-para-xylylene (Parylene-C; red area). The 32-channel electrode tips were arranged in a regular grid (50 μm \times 50 μm with a 0.4 mm inter-electrode distance). Electric signals were delivered by gold wires (20- μm wide; yellow lines) that were covered with Parylene-C. A silicon probe electrode was inserted through the mesh hole (asterisk) at the center of the ECoG array. In this sketch view, electrode tips were exposed on the inferior surface (see B). Inset: The size of individual electrodes the center-to-center distances between adjacent electrodes, and the center-to-center and side-to-side distances between adjacent holes. Black and blank squares were electrode and hole in the array. (B) A schematic drawing of the formation of electrodes on the surface of the barrel cortex. Electrophysiological signals from all layers of the rat barrel cortex were recorded by a 32-channel silicon probe (length \sim 1.6 mm; green, black squares indicate the individual electrode tips). (C) Whisker stimulation. Individual whiskers of anesthetized rats were moved by piezoelectric actuators with unidirectional micro-movements. Stimulation to the individual whisker was achieved by a photoMOS switch controlled by a personal computer. A conventional interface of the window of the personal computer helped to stimulate an arbitrary whisker. (D) Examples of simultaneously recorded traces of whisker-evoked responses from different electrodes of the ECoG array or the LFP probe. The top trace (a) is a driving signal to the piezoelectric actuator for whisker stimulation. The arrangement of the traces indicates the locations of electrodes in the ECoG array (b–e) and the silicon probe electrodes (f–i) from the brain surface (depth 0.1 mm) to the intermediate layer (depth 0.7 mm) of the cortex.

delay δ to LFP at depth d . The time delay δ was taken from 1 ms to $T=26$ ms. N is the number of used ECoG channels for regression.

The weight coefficient was determined from the training datasets through SLiR algorithm that imposed the sparse conditions by using the automatic relevance determination (ARD) prior. In particular, SLiR imposed sparse conditions only for the channel dimension, and not for the temporal dimension (see Toda et al., 2011, for detailed explanation). By applying the variational Bayesian method, SLiR iteratively estimated the weights and the ARD parameters, which represented how much the weight contributes to the reconstruction. Based on the values of the estimated ARD parameters, the relevant channels were automatically selected and irrelevant channels were discarded.

During the construction (training) process of the weight coefficient, ECoG signals in a temporal window of -26 to -1 ms (past) were used to reconstruct the LFP signals at time 0.

The temporal window of 25 ms was determined through analysis in preliminary experiments, in which the 25 ms time window was found to provide the highest performance of the reconstruction. The reconstruction process was performed at each time point t (1 ms step) of the data. LFP signals were reconstructed from all or a part of the preceding ECoG signals ($N=1, 4$ or 32).

Throughout our study, a dataset of spontaneous cortical activities was used to compute the weight coefficients. In a given recording session of spontaneous cortical activity in each subject, the initial 10 datasets (2 s each) were used for training, and the following 49 datasets were used for testing reconstruction accuracy. Reconstructions using the weight coefficients were performed for each single recording session in both the spontaneous and evoked LFPs. Reconstruction accuracy was quantified using the correlation coefficient (R) between the real and reconstructed LFPs. The reconstruction accuracies were expressed as means \pm standard error of the data of each trial, unless otherwise mentioned.

2.6. Time frequency analysis

To assure the error estimation of individual frequency-components with time variable in reconstructed LFPs, time frequency analyses were performed using short-time discrete fast Fourier transform with a sliding window. Sliding windows 0.25 s wide with a 12.5 ms overlap were used to compute a baseline spectrogram from 0.25 s before and after the stimulus onset, in the 0–300 Hz range. In the time frequency analysis, Hamming window was used as a window function.

2.7. Current source density (CSD) analysis

LFP traces are often attributable to the volume conduction from remote current generators (Nicholson and Freeman, 1975; Mitzdorf, 1985). Thus, voltage traces are not always reliable for tracing the structural sources of the field events. CSD analysis provides a more precise localization of the origin of extracellular currents (Nicholson and Freeman, 1975; Mitzdorf, 1985). When extracellular potentials are measured simultaneously at various depths, the CSD derives from the voltage traces enables continuous monitoring of the exact anatomical locations of current sinks and sources.

The continuous spatial distributions of sinks and sources were calculated from the spatially sampled electric potentials. The CSD profile was obtained by following the second spatial derivative, $\{x_{i-1}(t) + x_{i+1}(t) - 2x_i(t)\}/d^2$, where $x_i(t)$ is the LFP signal of channel i at time t and d is the inter-electrode distance. The LFP channel indices were assigned in an ascending order of the electrode locations from the cortical surface to deep layers. Before conducting the CSD analysis, raw LFPs were low-pass filtered using a Butterworth filter with a cutoff frequency of 250 Hz. Spatiotemporal depth

profiles of the CSDs were obtained with a spatial Gaussian filter to reduce the noise.

2.8. Histology

At the end of each experiment, the deeply anesthetized rat (intraperitoneally pentobarbital administration; 80 mg/kg) was transcardially perfused with 0.9% saline followed by 10% formalin. The brain was removed and post-fixed in 10% formalin solution for several days. Serial coronal sections (50 μ m) were cut through the area of interest with a vibratome (DTK-2000; Dosaka EM Co., Ltd, Kyoto, Japan) and were Nissl-stained for identification of the barrel field and cortical layers. The tracks of the silicon probe electrode in the barrel cortex were fully identified in the fixed cortical tissue. The tips of the recording probes were positioned at the layer 6 of the barrel cortex.

3. Results

3.1. Reconstruction of spontaneous LFPs from spontaneous ECoG signals

Fig. 2A and B shows simultaneously recorded, spontaneous, 32-channel ECoG and 32-channel LFP signals in the barrel cortex of a urethane-anesthetized rat. Examples of simultaneously recorded ECoG and intracortical LFP signals from one of these channels are shown in Fig. 3A and B (black trace), respectively. The red trace in Fig. 3B shows the LFP signal reconstructed using an SLiR from simultaneously recorded 32-channel ECoG signals. Fig. 3C shows the high accuracy of the reconstruction ($R=0.931$). Time-frequency analyses of real LFPs (Fig. 3D) and reconstructed LFPs (Fig. 3E) revealed that the reconstructed LFPs exhibited a distribution of individual frequency components similar to the real LFPs, suggesting that the SLiR enabled a successful reconstruction of the intracortical LFPs from the 32-channel ECoG signals.

3.2. Depth profiles of real and reconstructed LFPs

Throughout the reconstruction process, the question arose as to whether the LFP signals reconstructed from ECoG signals carried physiologically meaningful information. To address this question directly, we conducted CSD analyses of the reconstructed LFPs. Large amplitude positive or negative spontaneous LFP components were recorded from intermediate to deep layers of the cortex (Fig. 2B and C). CSD analysis revealed that sinks in the superficial layer (depth 0.20–0.50 mm) were consistently coupled with source responses in the intermediate layer (depth 0.55–0.80 mm; Fig. 2D). The sinks were related to occurrences of large negative deflections of LFPs from the deeper part of the superficial layer to the intermediate layer (Fig. 2C). Reconstructions of LFPs at various depths yielded a high accuracy of reconstruction ($R=0.92 \pm 4.3 \times 10^{-3}$) (Fig. 2E and F). The spatiotemporal profile of current sinks calculated from the reconstructed LFPs was similar to the CSD profile obtained from the real LFPs (Fig. 2G). These results suggested that LFPs reconstructed with the SLiR carried physiological information about the signal processing in the barrel cortex.

3.3. Single-trial reconstruction of LFPs in response to whisker stimulation using a weight coefficient from the spontaneous activity

After recording the spontaneous activity, we also conducted simultaneous multichannel recordings of ECoGs and intracortical LFPs during the responses to repetitive stimulation of the whiskers. Rats were exposed to repetitive deflection of a single whisker by a piezoelectric-driven actuator (Fig. 4A). Evoked responses were

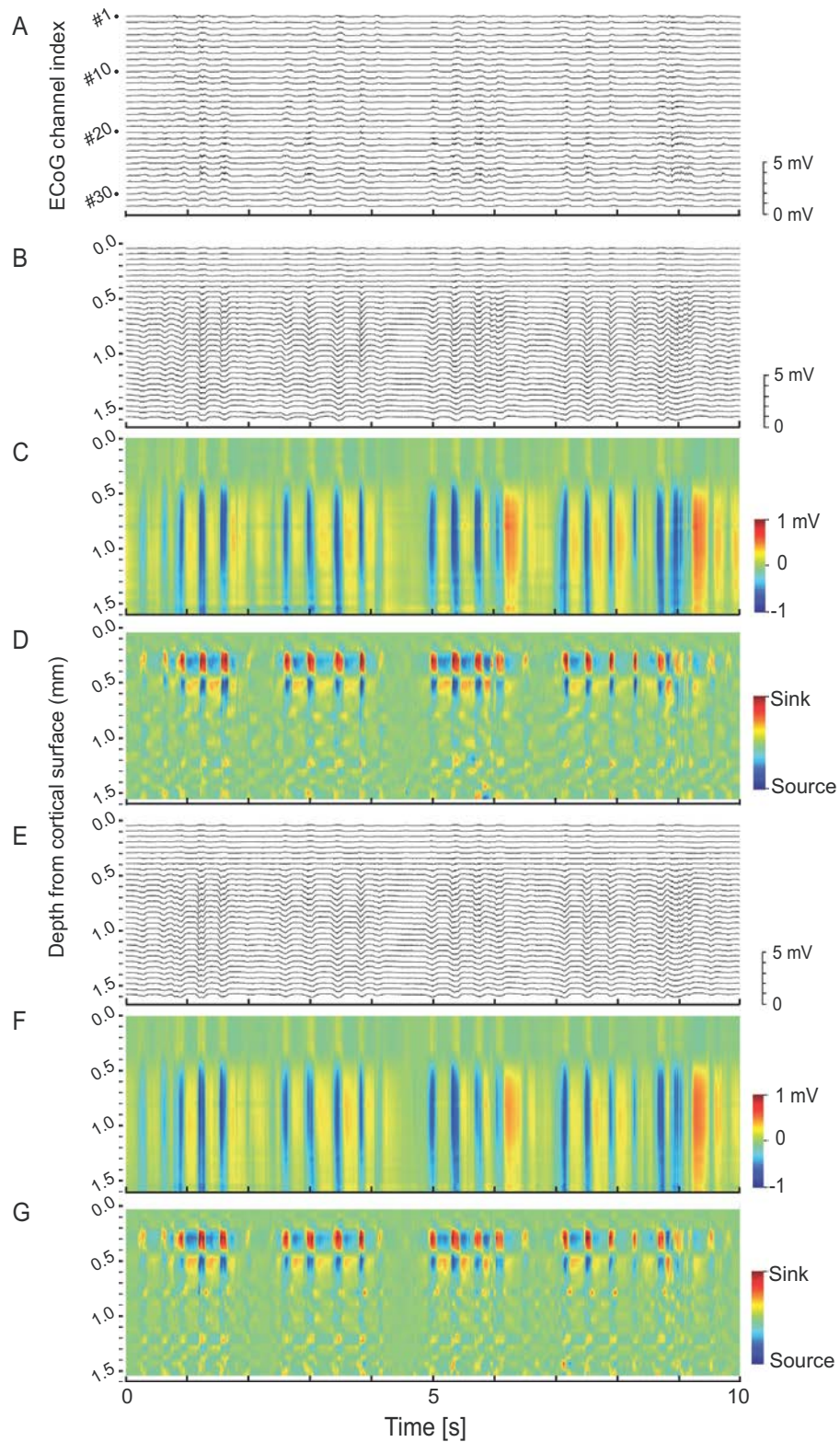


Fig. 2. Reconstruction of spontaneous LFPs. (A) Example of spontaneous ECoG signals. The traces from top to bottom were associated with ascending order of the channel index, as shown in Fig. 1A. (B) Depth profile of real LFPs recorded from the silicon probe electrode. The traces from top to bottom were recorded at various depths from the cortical surface to the deep layer in the barrel cortex. Each recording depth was separated by $50\ \mu\text{m}$ from the adjacent channel. (C) Color-coded illustration of depth profile of real LFP amplitudes. (D) Color-coded illustration of depth profile of real CSDs. (E) Depth profile of reconstructed LFPs. Reconstruction of LFPs was calculated from the simultaneously recorded ECoG signals in A. (F) Color-coded illustration of depth profile of reconstructed LFP amplitudes. (G) Color-coded illustration of depth profile of CSDs obtained from the reconstructed LFPs.

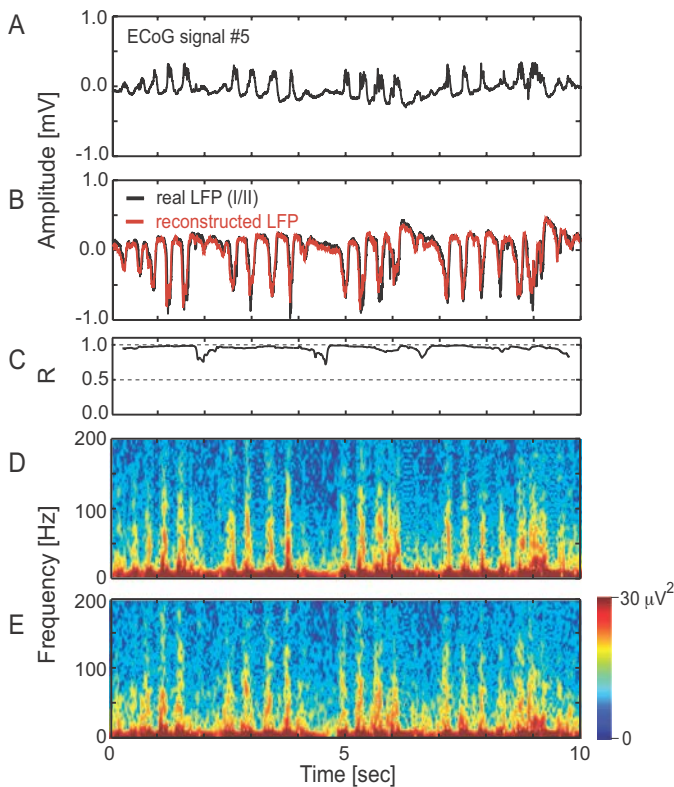


Fig. 3. Examples of simultaneously recorded spontaneous signals. (A) Spontaneous ECoG signals recorded from electrode #5 (corresponding to the index in Fig. 1A) in the rat barrel cortex. (B) LFPs (black trace) recorded from the superficial cortical layer II/III and the LFP (red trace) reconstructed from the 32-channel ECoG signals. This reconstructed LFP appeared similar to the real LFP in B. (C) Temporal profile of the correlation coefficient between the real LFP and reconstructed LFP. The correlation coefficients were calculated using a sliding window of 500 ms moving in steps of 2 ms. The correlation coefficient between these two profiles of LFPs was 0.931. (D, E) Time-frequency analyses of real LFP (D) and reconstructed LFP (E). Color coding represents the power of the signals.

recorded across the ECoG and intracortical LFP electrodes following individual stimuli (Fig. 4B–F).

Analyses of the CSD profiles indicated that there were dominant current sink and source complexes (Fig. 4E and G) following individual whisker stimulations. A characteristic sink-source pattern was observed in the superficial and intermediate layers. The sink was initiated in the superficial layer and was accompanied by a source in the intermediate layer. The sink duration, which was determined by bandwidth at half maximum of the CSD profile, was 72 ± 55 ms. The secondary current sinks were successively observed in the intermediate layer. The CSD profile during whisker stimulation was similar to that during the resting state.

To evaluate the preservation of relationships between ECoG signals and intracortical LFPs during spontaneous neural activity, weight coefficients calculated from the dataset of spontaneous activity were applied to the ECoG signals in the dataset of the stimulus-evoked responses to reconstruct the evoked LFPs. LFPs were also successfully reconstructed from the ECoGs in this case (Fig. 4H, J, and see solid lines in Fig. 5B). We found that, even at a depth of 1.5 mm from the cortical surface (corresponding to the upper part of layer VI), depth profiles of LFPs were successfully reconstructed from ECoGs with high accuracy ($R > 0.9$, see solid lines in Fig. 5B).

The spatiotemporal profiles of the current sinks and sources in the barrel cortex represented by the reconstructed LFPs were similar to those of the real LFPs (Fig. 4I and K). The short latency sinks

derived from the reconstructed LFPs were detected in the superficial layer immediately following the whisker stimuli. The sinks were then attenuated and successively shifted to the intermediate layer. These features seemed to be due to activities of neural populations in each layer through synaptic inputs with various latencies (Armstrong-James et al., 1992), and were similar to the spatiotemporal features of the CSDs reconstructed from the real LFPs (Fig. 4E and G). Together, these results suggest that the circuit operation of the barrel cortex during the spontaneous bursting was at least partly common with that during responses to the whisker stimuli in urethane-anaesthetized rats.

3.4. Performance of reconstruction depends on the number of ECoG channels

To assess the dependence of the reconstruction accuracy of intracortical LFPs on the number of ECoG channels, subsets of ECoG electrode channels were selected and used to reconstruct the LFPs using a weight coefficient constructed during the spontaneous activity (Fig. 5A). The four channels around the LFP electrode still enabled relatively high accuracy ($R > 0.7$) reconstruction across various depths (Fig. 5B, dotted line), although some decline in accuracy was observed below the depth 0.5 mm. Reconstruction from only one ECoG channel signal was made with high accuracy ($R > 0.7$) only in the superficial layer (above the depth of 0.3 mm), while below a depth of 0.5 mm the reconstruction accuracy declined ($R \approx 0.4$). These results suggest that generalization of the relationships between spontaneous ECoG signals and intracortical LFPs was maintained across different brain states, and that better reconstructions, especially of the deeper layer LFPs, require larger number of ECoG channels.

4. Discussion

We recorded spontaneous activity and whisker-evoked responses from the barrel cortex of urethane-anaesthetized rats using simultaneous recordings with 32-channel ECoG and 32-channel LFP electrodes. SLiR analysis enabled us to successfully reconstruct LFPs from spontaneous ECoG signals with high accuracy. The weight coefficients derived through the SLiR to reconstruct the LFPs from ECoG signals during the spontaneous state, was then applied to reconstruct the whisker-evoked LFP responses. The CSD profiles obtained from the reconstructed LFPs matched those derived from real LFPs. These results demonstrated that the relationship between intracortical and cortical-surface signals was shared across the spontaneous bursting and stimulus-evoked neural activity in the barrel cortex of urethane-anaesthetized rats.

In the present study, for the first time, we showed that the relationship (weight coefficient) between LFPs and ECoGs was preserved across different brain states. In Figs. 2D and 4G, the CSD profile during whisker stimulation was similar to that during resting state. The results suggested that common neural circuits were operating during both of spontaneous burst and whisker-evoked responses. The major component of the weight coefficient might reflect the physical electric conduction within the cerebral cortical tissue, because the reconstruction process was performed on the data at each time point. However, we set a temporal window of 25 ms (past) for constructing (learning) the weight coefficient to reconstruct the LFPs from the ECoG signals. Moreover, reductions in the reconstruction accuracy along the depth profile did not seem to be uniform; as shown in Fig. 5B, the reconstruction accuracy was rather constant at cortical layers deeper than 0.7 mm, while the notch was observed at depth 0.5 mm. Such the depth-dependence of reconstruction accuracy of deep layer LFPs was corresponded with one in the motor cortex of awake

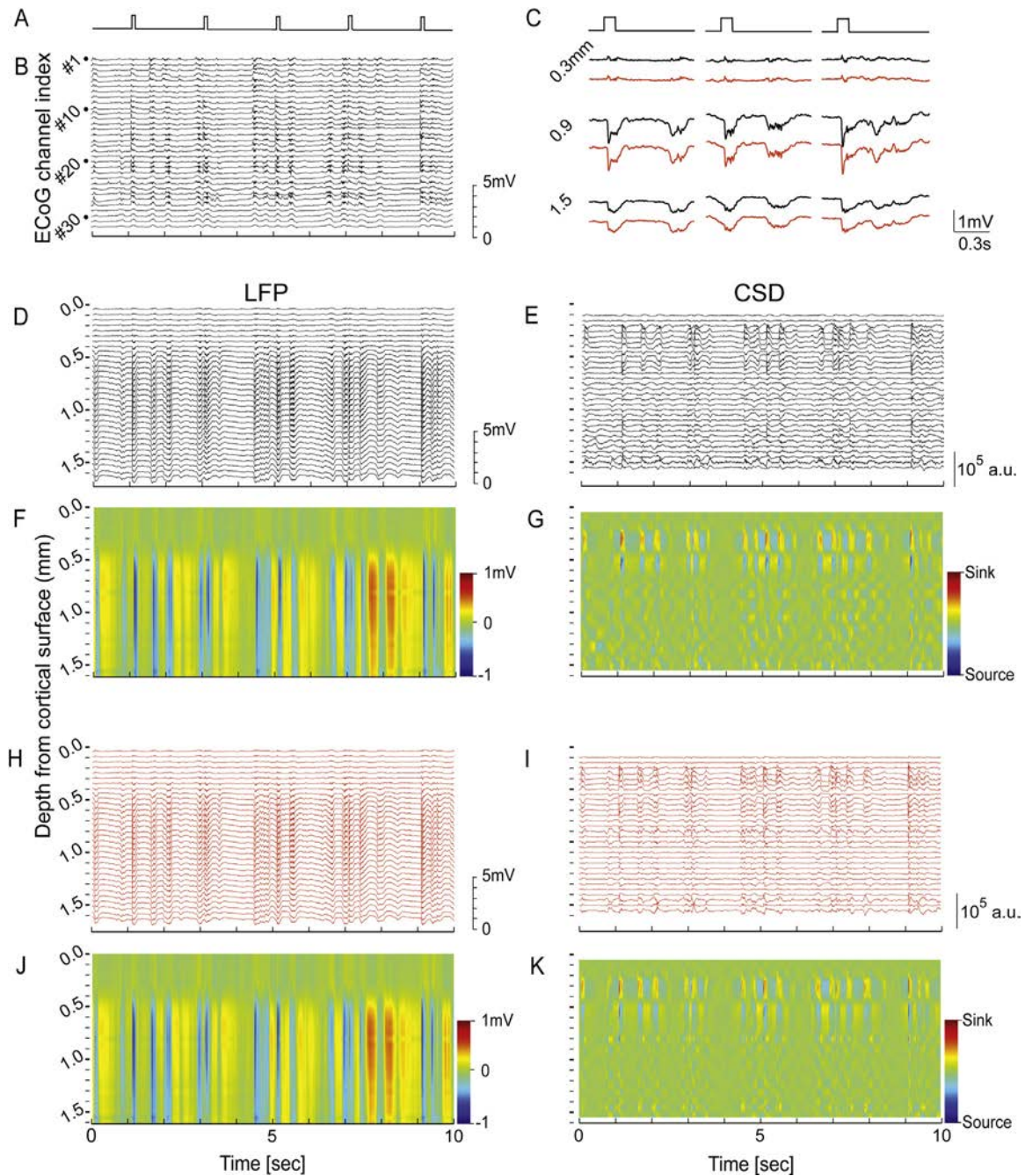


Fig. 4. Reconstruction of whisker-evoked LFPs. (A) Voltage trace of piezoelectric actuators for whisker stimulation. (B) Simultaneously recorded signals in the ECoG array. The traces from top (#1) to bottom (#32) corresponds to the channel index shown in Fig. 1A. (C) Three typical responses of real (black trace) and reconstructed (red trace) whisker-evoked LFPs at depths of 0.3, 0.9, and 1.5 mm from the cortical surface. Timings of whisker stimulation are indicated as square pulses on the top voltage trace. (D–G) Temporal profiles of real LFPs (D and F) and CSDs (E and G). (H–K) Temporal profiles of reconstructed LFP (H and J) and CSDs (I and K). The color bars in F, J and G, K indicate amplitudes of LFPs and current, respectively.

monkey (Watanabe et al., 2012; the downward trend was not observed below a depth of approximately 0.8 mm). In the previous study of ours, neural network dynamics were reflected in the weight coefficient for estimating the LFPs from the ECoG signals. Thus, the weight coefficients between ECoG and LFP signals in the present experiments may involve the neural dynamics of cortical circuits as well as the electric conduction properties.

Amplitude and polarity of the LFPs are modulated in accordance with the depth of recordings in the cortex (e.g., Richardson et al., 1987; Di et al., 1990), the so-called depth modulation. The depth modulation of LFPs is caused by laminar-specific

synaptic input and the balance of current source and sinks in the main shafts of apical dendrites of principal cells. While reversed polarity of the LFPs relative to the depth of recording locations was not clearly observed in our data, the CSD analysis clearly revealed synaptic events within the barrel column. Prominent sinks following whisker stimulation were characterized in the deeper part of the superficial layer, corresponding to layer II/III. The current sink persisted for approximately 70 ms as judged from the half width. Following the sink, a current source appeared in the superficial layer. The initial current sink profile was assumed to be the result of monosynaptic thalamic input (Zhang and Deschenes,

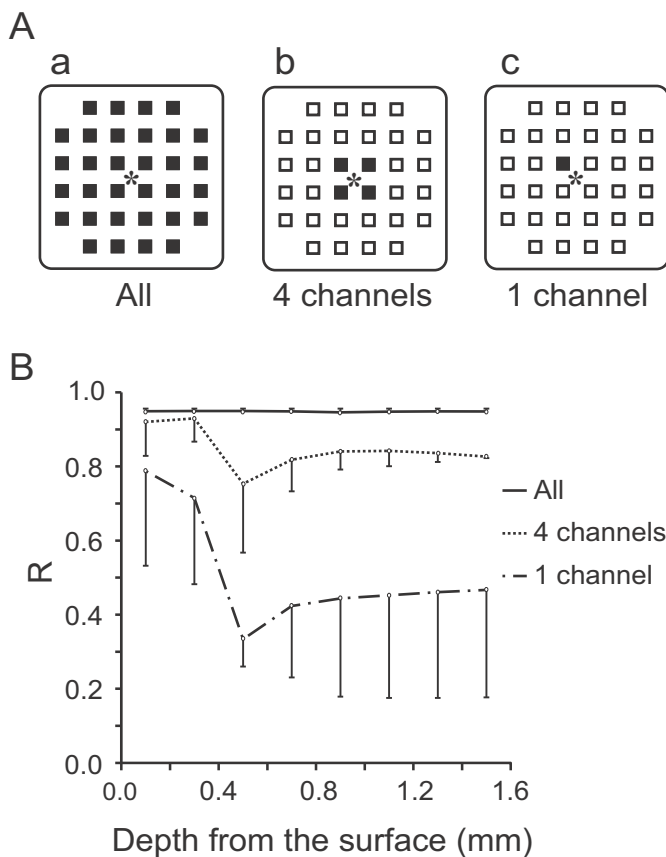


Fig. 5. Accuracy of LFP reconstruction from subsets of ECoG channels. (A) Variations in ECoG-channel subsets used for reconstruction of LFPs. Real LFPs were recorded from the center of the ECoG array (asterisk). The subsets of ECoG channels (filled squares) consisted of 32 (a), 4 (b), or 1 (c) ECoG channels. (B) Relationship between the reconstruction accuracies and depth of the LFP recordings from the cortical surface for the various subsets of ECoG channels shown in A. The interval of reconstructed LFPs was 0.2 mm. Error bars indicate standard errors across trials in the dataset.

1998). The transition of prominent sink-sources in layer II/III after whisker stimulation was consistent with previous findings in the rat barrel cortex (Di et al., 1990) and the somatosensory cortex (Toth et al., 2008), although the durations of the sinks after stimulation were shorter in the previous findings than those in our current data. In contrast to previous reports of CSD analyses (Di et al., 1990; Minlebaev et al., 2007; Toth et al., 2008), the source responses occurred in the intermediate layer, corresponding to layer IV, and were consistently coupled with the current sinks in the superficial layer. Our CSD analyses revealed characteristic laminar-specific synaptic events within the barrel column from both the real and reconstructed LFPs. A detailed spatiotemporal profile of the CSDs during spontaneous activity and whisker-evoked responses should be examined in the future.

Kinematics and kinetics of arm movements, or neural responses to sensory inputs were decoded from ECoG signals in various cortical areas. The decoding accuracy depends on the design of the ECoG array such as the appropriate electrode arrangement in the brain, their number, size and impedance (Waldert et al., 2009). However, it is difficult to judge which parameter principally contributes to maximum achievement of the decoding accuracy. The optimal inter-electrode distance is also elusive. In experiments on anesthetized rats, spatial frequency analysis estimated the optimal inter-electrode distance of subdural electrodes to be 0.6 mm (Slutzky et al., 2010). For estimation of intracortical LFPs in the rat barrel cortex in the present study, we used the ECoG array with

an inter-electrode distance of 0.4 mm. A subset of four neighboring ECoG signals in our ECoG array was capable of reconstructing LFPs with relatively high accuracy ($R > 0.7$ in layer III), while nearly full reconstruction of the LFPs in the deep layer was possible ($R > 0.9$) from all the 32 channels (Fig. 5B). Systematic study is still needed to determine the best parameter of the ECoG array design depending on the purpose of its usage, such as BMI, clinical application, or estimation of intracortical neural signals.

In this experiment, we studied the shared relationship of neural signals between responses to peripheral stimulations and spontaneous activities under urethane anesthesia. Comparative analyses among different brain states, including other anesthetic drugs or under awake conditions, are required for revealing the neural processing occurring in intrinsic circuits under different conditions. The relationships of multiple neural activities unraveled by such analyses will be a basis for the general concept of neural representation.

Acknowledgements

This study was supported by a 'Brain Machine Interface Development' program carried out under the Strategic Research Program for Brain Sciences from the Ministry of Education, Culture, Sports, Science, and Technology of Japan. We thank K. Isa (NIPS) for general support, and O. Yamashita (ATR), J. Morimoto (ATR), and K. Toyama (ATR) for their helpful discussions. Part of this research was supported by the National Institute of Information and Communications Technology.

References

- Armstrong-James, M., Fox, K., Das-Gupta, A., 1992. Flow of excitation within rat barrel cortex on striking a single vibrissa. *J. Neurophysiol.* 68, 1345–1358.
- Chen, C., Shin, D., Watanabe, H., Nakanishi, Y., Kambara, H., Yoshimura, N., Nambu, A., Isa, T., Nishimura, Y., Koike, Y., 2013. Prediction of hand trajectory from electrocorticography signals in primary motor cortex. *PLOS ONE* 8, e83534.
- Crone, N.E., Hao, L., Hart Jr., J., Boatman, D., Lesser, R.P., Irizarry, R., Gordon, B., 2001. Electrocorticographic gamma activity during word production in spoken and sign language. *Neurology* 57, 2045–2053.
- Crone, N.E., Miglioretti, D.L., Gordon, B., Sieracki, J.M., Wilson, M.T., Uematsu, S., Lesser, R.P., 1998. Functional mapping of human sensorimotor cortex with electrocorticographic spectral analysis. I. Alpha and beta event-related desynchronization. *Brain* 121, 2271–2299.
- Di, S., Baumgartner, C., Barth, D.S., 1990. Laminar analysis of extracellular field potentials in rat vibrissa/barrel cortex. *J. Neurophysiol.* 63, 832–840.
- Edwards, E., Soltani, M., Deouell, L.Y., Berger, M.S., Knight, R.T., 2005. High gamma activity in response to deviant auditory stimuli recorded directly from human cortex. *J. Neurophysiol.* 94, 4269–4280.
- Freeman, W.J., Baird, B., 1987. Relation of olfactory EEG to behavior: spatial analysis. *Behav. Neurosci.* 101, 393–408.
- Fukushima, M., Saunders, R.C., Leopold, D.A., Mishkin, M., Averbeck, B.B., 2012. Spontaneous high-gamma band activity reflects functional organization of auditory cortex in the awake macaque. *Neuron* 74, 899–910.
- Katzner, S., Nauhaus, I., Benucci, A., Bonin, V., Ringach, D.L., Carandini, M., 2009. Local origin of field potentials in visual cortex. *Neuron* 6, 35–41.
- Krupa, D.J., Brisben, A.J., Nicolelis, M.A., 2001. A multi-channel whisker stimulator for producing spatiotemporally complex tactile stimuli. *J. Neurosci. Methods* 104, 199–208.
- Lachaux, J.P., George, N., Tallon-Baudry, C., Martinerie, J., Hugueville, L., Minotti, L., Kahane, P., Renault, B., 2005. The many faces of the gamma band response to complex visual stimuli. *Neuroimage* 25, 491–501.
- Lindén, H., Tetzlaff, T., Potjans, T.C., Pettersen, K.H., Grün, S., Diesmann, M., Einevoll, G.T., 2011. Modeling the spatial reach of the LFP. *Neuron* 72, 859–872.
- Majima, K., Matsuo, T., Kawasaki, K., Kawai, K., Saito, N., Hasegawa, I., Kamitani, Y., 2014. Decoding visual object categories from temporal correlations of ECoG signals. *Neuroimage* 90, 74–83.
- Miller, K.J., Zanos, S., Fetz, E.E., den Nijs, M., Ojemann, J.G., 2009. Decoupling the cortical power spectrum reveals real-time representation of individual finger movements in humans. *J. Neurosci.* 29, 3132–3137.
- Minlebaev, M., Ben-Ari, Y., Khazipov, R., 2007. Network mechanisms of spindle-burst oscillations in the neonatal rat barrel cortex in vivo. *J. Neurophysiol.* 97, 692–700.
- Mitzdorf, U., 1985. Current source-density method and application in cat cerebral cortex: investigation of evoked potentials and EEG phenomena. *Physiol. Rev.* 65, 37–100.

- Nambu, I., Osu, R., Sato, M.A., Ando, S., Kawato, M., Naito, E., 2009. Single-trial reconstruction of finger-pinch forces from human motor-cortical activation measured by near-infrared spectroscopy (NIRS). *Neuroimage* 47, 628–637.
- Nicholson, C., Freeman, J.A., 1975. Theory of current source-density analysis and determination of conductivity tensor for anuran cerebellum. *J. Neurophysiol.* 38, 356–368.
- Ray, S., Niebur, E., Hsiao, S.S., Sinai, A., Crone, N.E., 2008a. High-frequency gamma activity (80–150 Hz) is increased in human cortex during selective attention. *Clin. Neurophysiol.* 119, 116–133.
- Ray, S., Crone, N.E., Niebur, E., Franaszczuk, P.J., Hsiao, S.S., 2008b. Neural correlates of high-gamma oscillations (60–200 Hz) in macaque local field potentials and their potential implications in electrocorticography. *J. Neurosci.* 28, 11526–11536.
- Richardson, T.L., Turner, R.W., Miller, J.J., 1987. Action-potential discharge in hippocampal CA1 pyramidal neurons: current source-density analysis. *J. Neurophysiol.* 58, 981–996.
- Paxinos, G., Watson, C., 2007. *The Rat Brain in Stereotaxic Coordinates*, 6th ed. Academic Press, San Diego.
- Shin, D., Watanabe, H., Kambara, H., Nambu, A., Isa, T., Nishimura, Y., Koike, Y., 2012. Prediction of muscle activities from electrocorticograms in primary motor cortex of primates. *PLOS ONE* 7, e47992.
- Slutzky, M.W., Jordan, L.R., Krieg, T., Chen, M., Mogul, D.J., Miller, L.E., 2010. Optimal spacing of surface electrode arrays for brain-machine interface applications. *J. Neural Eng.* 7, 26004.
- Toda, H., Suzuki, T., Sawahata, H., Majima, K., Kamitani, Y., Hasegawa, I., 2011. Simultaneous recording of ECoG and intracortical neuronal activity using a flexible multichannel electrode-mesh in visual cortex. *Neuroimage* 54, 203–212.
- Toth, A., Gyengesi, E., Zaborszky, L., Detari, L., 2008. Interaction of slow cortical rhythm with somatosensory information processing in urethane-anesthetized rats. *Brain Res.* 1226, 99–110.
- Trautner, P., Rosburg, T., Dietl, T., Fell, J., Korzyukov, O.A., Kurthen, M., Schaller, C., Elger, C.E., Boutros, N.N., 2006. Sensory gating of auditory evoked and induced gamma band activity in intracranial recordings. *Neuroimage* 32, 790–798.
- Waldert, S., Pistohl, T., Braun, C., Ball, T., Aertsen, A., Mehring, C., 2009. A review on directional information in neural signals for brain-machine interfaces. *J. Physiol. Paris* 103, 244–254.
- Watanabe, H., Sato, M.A., Suzuki, T., Nambu, A., Nishimura, Y., Kawato, M., Isa, T., 2012. Reconstruction of movement-related intracortical activity from micro-electrocorticogram array. *J. Neural Eng.* 9, 036006.
- Yanagisawa, T., Hirata, M., Saitoh, Y., Goto, T., Kishima, H., Fukuma, R., Yokoi, H., Kamitani, Y., Yoshimine, T., 2011. Real-time control of a prosthetic hand using human electrocorticography signals. *J. Neurosurg.* 114, 1715–1722.
- Yanagisawa, T., Hirata, M., Saitoh, Y., Kishima, H., Matsushita, K., Goto, T., Fukuma, R., Yokoi, H., Kamitani, Y., Yoshimine, T., 2012a. Electrocorticographic control of a prosthetic arm in paralyzed patients. *Ann. Neurol.* 71, 353–361.
- Yanagisawa, T., Yamashita, O., Hirata, M., Kishima, H., Saitoh, Y., Goto, T., Yoshimine, T., Kamitani, Y., 2012b. Regulation of motor representation by phase-amplitude coupling in the sensorimotor cortex. *J. Neurosci.* 32, 15467–15475.
- Yazdan-Shahmorad, A., Kipke, D.R., Lehmkuhle, M.J., 2013. High gamma power in ECoG reflects cortical electrical stimulation effects on unit activity in layers V/VI. *J. Neural Eng.* 10, 066002.
- Zhang, Z.W., Deschenes, M., 1998. Projections to layer VI of the posteromedial barrel field in the rat: a reappraisal of the role of corticothalamic pathways. *Cereb. Cortex* 8, 428–436.